Electromagnetic Analysis of the Updated Fast Control Coil for EAST

Xianewei Wang[1], Zhaoliang Wang[2], Fei Xie[3], Qing He[1], Xiulian Li[1], Wentao Xie[1]
[1]Jiangsu University of Technology, Changzhou 213001, China. E-mail: wangxw@jsut.edu.cn, qqaa611@163.com, 936303415@qq.com, 790887443@qq.com
[2]Institute of Plasma Physics, Chinese Academy of Sciences, Hefei 230031, China. E-mail: zhlwang@ipp.ac.cn
[3]Shunde Polytechnic, Foshan 528000, China. E-mail: jeffrey_xie@163.com

Fast control coil is one of the most important components for EAST device to control the vertical stability of plasma. However, once the heating power of EAST is updated to 36 MW, fast control coil doesn't adapt to the new operation state and couldn't provide effective control for plasma vertical instability. Thus, insulation material with ITER-like magnesium oxide is developed to withstand high radiation and the coil position is also relocated to obtain more effective instability control. Given the relocation of fast control coil, electromagnetic load acting on coil-self and feeders are calculated based on elliptical integral and Ampere force law. The electromagnetic load as volumetric force is interpolated into the finite element analysis model to analyze the stress state on fast control coil. Finally, the design-by-analysis method is adopted to evaluate whether the stress could satisfy the specified acceptance criteria. The study will provide theoretical reference for the update of fast control coil from the perspective of electromagnetic load.

Keywords: EAST, Fast Control Coil, Plasma, Magnetic Density, Design Stress Intensity

1 Introduction

The loss of vertical plasma position control will result in thermal load on plasma facing components and can lead to plasma disruption events, which cause large electromagnetic load and other undesirable consequences [1]. The position control of plasma can be partly achieved by poloidal magnetic coils. However, the poloidal coils are installed outside the vacuum vessel. Given the shielding delay of vacuum vessel for the magnetic field caused by poloidal magnetic coils, two sets of fast control coil were symmetrically arranged with respect to Experimental Advanced Superconducting Tokamak (EAST) middle plane in 2006 and were connected in anti-series in order to provide horizontal field for the fast control of plasma vertical motion [2, 3, 4].

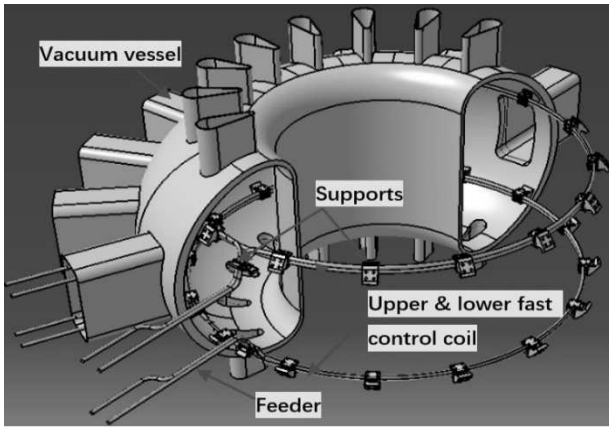

Fig. 1 *Arrangement of fast control coil in vacuum vessel*

The fast control coil was mounted behind first wall and divertor plates to avoid facing plasma directly and fixed to inner wall of vacuum vessel [5]. Before updating, the coil was designed with water cooling copper conductor, epoxy insulation and stainless steel jacket. Recently, EAST team has planned to update plasma heating power to 36 MW and plasma operations have demonstrated old fast control coil cannot provide effective control for plasma vertical instability. Thus, upgrading fast control coil to accommodate higher performance plasma operation requirement is imperative.

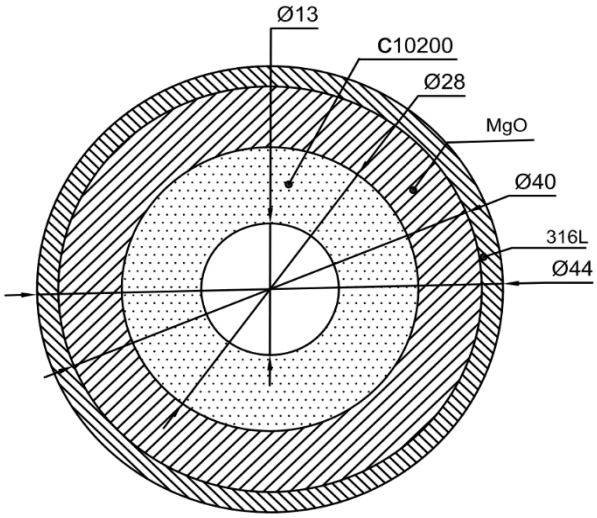

Fig. 2 *Dimension of fast control coil*

Fig. 1 shows the updated fast control coil, which includes a large arc segment and two feeders connected with the arc segment and led out through ports for leads and cooling pipe connection. For the updated fast control coil, high purity Magnesium Oxide (MgO) is adopted as the insulation material with a thickness of 6 mm as shown in Fig.2. MgO could withstand the radiation influence for EAST Tokamak (~1.3 MGy). Meanwhile, MgO can bear the highest baking temperature of 350° C in EAST vacuum vessel which is much lower than the melting point of 2852° C [6]. Besides the change of insulation material, fast control coil is relocated to a new position. Calculations have indicated plasma Vertical Displacement Event (VDE) growth rate reduced apparently when it is

relocated [7]. However, position change also leads to the variation of electromagnetic load acting on fast control coil. Therefore, it is necessary to analyze the mechanical state of fast control coil under electromagnetic force derived from magnet system and plasma current.

2 The electromagnetic calculation of the fast control coils

The fast control coil is in the complex back ground field, including the poloidal magnetic field, toroidal magnetic field, correctional magnetic field and the magnetic field caused by the plasma current. Thus, during the operation of EAST device, fast control will encounter large electromagnetic load. For the convenience of description electromagnetic force, we artificially divide the coil into two parts, namely the torus part and the feeder part. For the torus part, because its current direction is nearly parallel with the direction of magnetic field derived from toroidal field coil, therefore, the electromagnetic force caused by the interaction of fast control coil and toroidal field magnet is small. However, the current direction of fast control coil is almost perpendicular with the direction of magnetic field derived from poloidal field coil and plasma current, thus, the electromagnetic load generated by their interaction is very large. In addition, the saddle shaped correction coil and the picture frame edge localized mode coil will also result in certain electromagnetic force. Nevertheless, due to their specific shape and small current compared with the poloidal field coil and plasma current, the electromagnetic force caused by these coils is much smaller.

For the feeder part, by comparing its current direction with the directions of external magnetic field, we can conclude once EAST device is at the operation state, the feeder part will encounter huge electromagnetic force caused by toroidal field coil, poloidal field coil and plasma current. Meanwhile, there are also the electromagnetic force from correction coil and edge localized mode coil, but they are not very large. The detailed calculation of magnetic field and electromagnetic force is based on Maxwell equation. Given the specific shape of plasma, we use an equivalent model for its magnetic density calculation. Plasma current is discretized into circular charged filaments. We can calculate the magnetic density of discretized filaments and then use it to replace the magnetic density of plasma current. For a piece of charged circular filament, the magnetic density can be calculated as follow [8, 9].

$$B_r = \frac{-\mu_0 I Z}{2\pi\sqrt{Z^2+(r_0+r)^2}}[K(k) - \frac{Z^2+r_0^2+r^2}{Z^2+(r_0-r)^2}\cdot E(k)][T], \quad (1)$$

$$B_z = \frac{\mu_0 I}{2\pi\sqrt{Z^2+(r_0+r)^2}}[K(k) - \frac{Z^2-r_0^2+r^2}{Z^2+(r_0-r)^2}\cdot E(k)][T], \quad (2)$$

Where:

μ_0 …Vacuum permeability [-],

I… Current [A],

r_0… Large radius of filament [m],

r …Radial coordinate of an arbitrary point in the cylindrical coordinate system of filament [m],

Z…Axial coordinate of an arbitrary point in the cylindrical coordinate system of filament [m],

$K(k)$ …First kind elliptical integral [-]

$E(k)$ …Second kind elliptical integral [-].

The plasma current varies at different operation stage of EAST. And the current reaches peak value at the burnout stage. In our conservative analysis, the maximum value is adopted for the calculation of magnetic density. The magnetic field calculation of poloidal coils is also based on the method of elliptical integral. The toroidal coils and other irregular coils are divided into straight segments and arc segments to calculate the magnetic density respectively. The detailed calculation can be seen in references [10, 11, 12]. For the torus part of fast control coil, in view of symmetry of background field in the toroidal direction, we only need to focus on the distribution of background field at the cross section of fast control coil. Fig. 3 shows the variation of magnetic density on a 40° large arc segment. For the four pieces of feeder, since they have identical structure and are immersed in the same background field, we can choose an arbitrary feeder to calculate the magnetic density along its length direction. Fig. 4 shows the magnetic density on one feeder of the upper fast control coil.

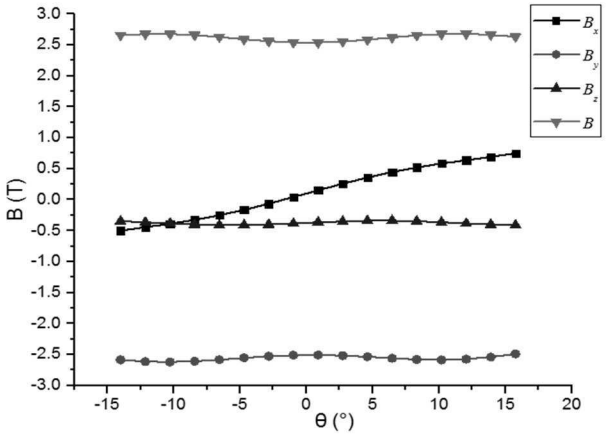

Fig. 3 *Magnetic density on the feeder*

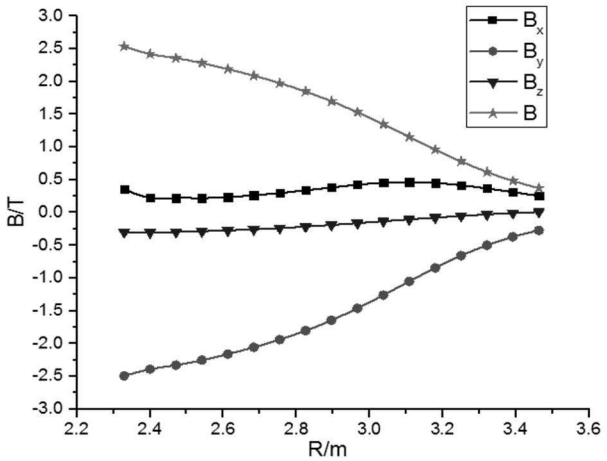

Fig. 4 *Magnetic density on the feeder*

Once the magnetic density has been calculated, combined with the current flowing through fast control coil, the electromagnetic force can be obtained based on Ampere force law. The distribution of electromagnetic force density on fast control coil is presented Fig. 5. The average electromagnetic force density on the torus segment is about 3700 Nm^{-1}. The minimum value on the feeder is at the potion far from the background coils and it is about 2600 Nm^{-1}. The corresponding peak value occurs at the oblique segment and it is about 24000 Nm^{-1}.

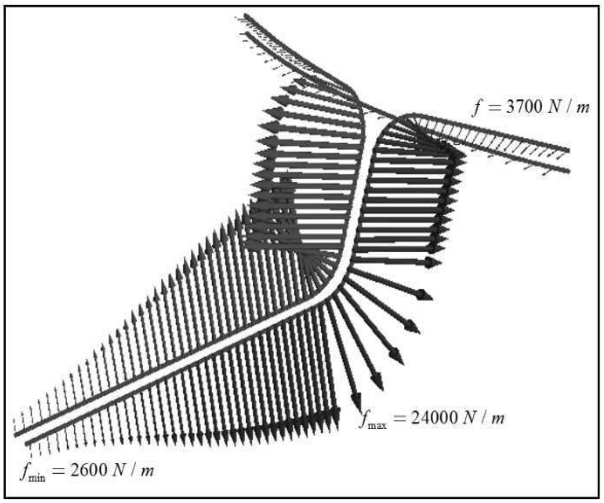

Fig. 5 *The electromagnetic force density on the large arc and feeder*

3 The finite element model and boundary conditions

Given the symmetrical arrangement of fast control coil with respect to EAST device, the distribution of magnetic density in the upper and lower fast control coil is similar. Thus, here we only select the upper fast control coil to carry out the study. In order to reduce the calculation workload of computer, the simulation model of upper fast control coil is divided into two parts, namely the large arc segment and feeder, which are analyzed individually. For the large arc segment, due to the approximate symmetry of its structure, one ninth large arc coil including the weakest supports is chosen to carry out mechanical analysis. Although the analysis with the weakest model is not the precise result of the real model, but the result will be conservative or safe to the structure. In addition, the analysis code (ANSYS 18.0) could compensate the remaining structure not-included-in simulation model under the cyclic symmetric boundary conditions. Two kinds of boundary condition are applied on the model shown in Fig. 6. The bottom of supporting rails is constrained with all degrees of freedom, because they are welded to the wall of vacuum vessel and this is a pretty good approximation. Cyclic symmetric constraint is a special type of restraint, which could be applied on a periodic structure to simplify the analysis model. Since the large arc segment can satisfy the constraint qualification, therefore, symmetric constraint is applied on the vertical cross section of the one ninth model.

For the feeders, since the distribution of electromagnetic force are nearly identical on different feeders, meanwhile, the configuration of different feeders is also alike, so we only need to select a piece of feeder to launch mechanical analysis. It should be pointed out that electromagnetic force declines quickly along feeder length direction, especially in the region outside the vacuum vessel. Thus，it is not necessary to build the entire feeder geometry model. The section in the penetration port is ignored in the analysis. In order to restrict the large deformation caused by external force, a series of clamps are mounted and bolted in the length direction. Considering the installation form and geometric structure, fixed and symmetric constraints are applied on feeder shown in Fig. 7.

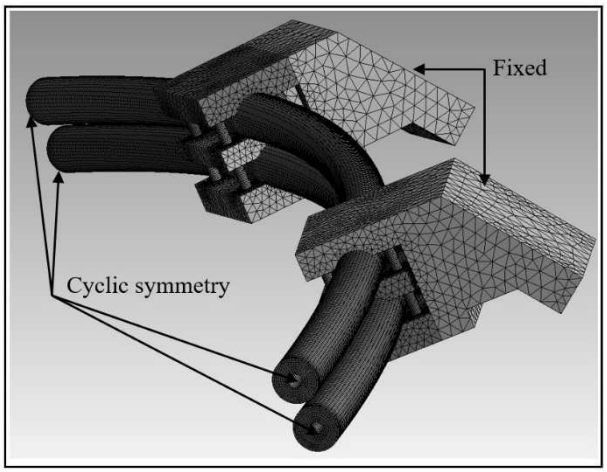

Fig. 6 *Constraints on the large arc*

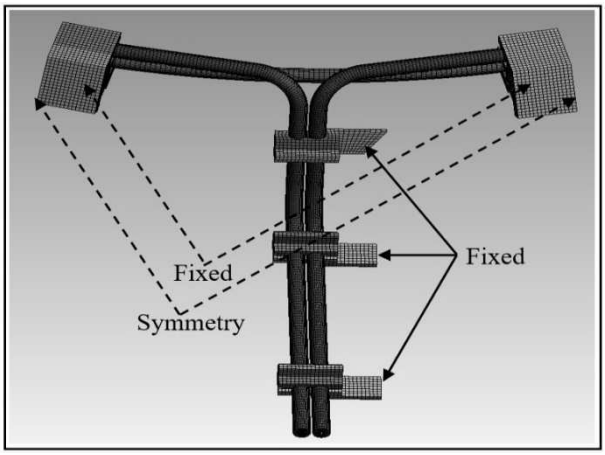

Fig. 7 *Constraints on the feeder*

4 Electromagnetic analysis and stress evaluation

Given the temperature rising of fast control coil caused by ohmic heat, the material property under the temperature of 100° C is adopted for the simulation. The detailed material property of fast control coil is listed in Tab. 1. Because the electromagnetic force is not a constant value but changing with spatial coordinate, it is applied on the finite element model in the form of functions for both the large arc and feeder, which can be easily realized by using ANSYS code. The simulation results demonstrate that the sum deformation of fast control coil

caused by electromagnetic fore is very small, which will not lead to structural failure or interfering with other components. The equivalent stress on the copper and the shear stress on the MgO are also very small, so they are not presented in the paper. The stress distribution of the large arc segment and feeder are listed in Fig. 8 and Fig. 9 respectively. For the large arc segment, the maximum equivalent stress occurs at the conductor jacket near to the region of support rail and the value is about 82 MPA. The stress in the other position is relatively smaller. For the feeder, the maximum stress also appears on the conductor jacket and the peak value is 190 MPA, which is resulted from stress concentration.

Tab. 1 *Properties of fast control coil at 100° C*

Property	Cu	MgO	316L	Unit
Young's modulus	1.14e11	9.6e8	1.93e11	Pa
Shear modulus	-	2.5e6	-	Pa
Poission's ratio	0.33	0.3	0.3	-
Density	8903	2200	7899	$Kg \cdot m^{-3}$

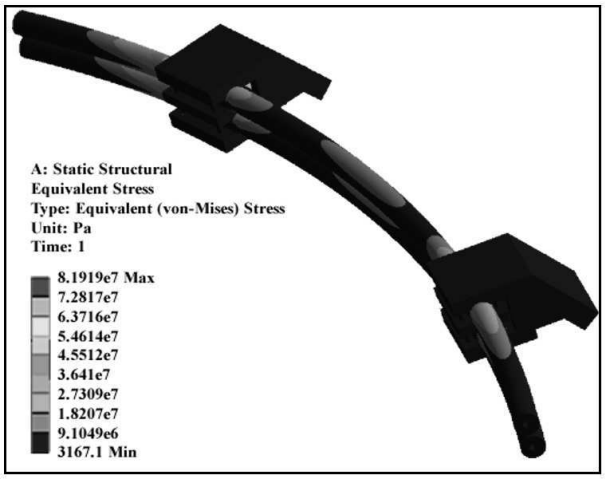

Fig. 8 *Equivalent stress on the large arc segment*

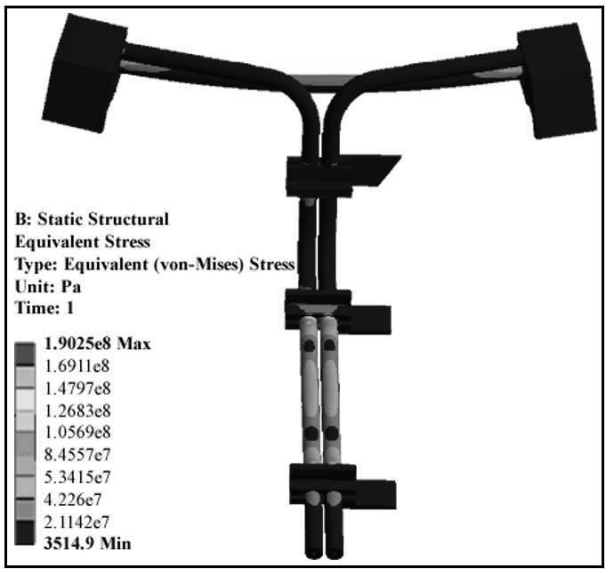

Fig. 9 *Equivalent stress on the feeder*

The stress evaluation of fast control coil is performed based on the design-by-analysis method specified in ASME Section VIII Div. 2 Part 5 [13，14，15，16]. According to the design-by-analysis method, stresses are classified into various types and different stress acceptance criteria are used for the peculiar stresses, which is shown in Tab. 2. According to the qualification shown in table 2, The bending stress caused by electromagnetic load and the local membrane stress near the support rails are not allowed to beyond the threshold of 221 MPA. Obviously, both the stress on the large arc and feeder are within the threshold.

Tab. 2 *The limit of stress intensity for jacket*

Type	Symbol	Limitation	Threshold (MPA)
Primary general membrane stress	S_I	S_m	147
Primary local membrane stress	S_{II}	$1.5\,S_m$	221
Primary membrane plus bending stress	S_{III}	$1.5\,S_m$	221
Primary stress plus second stress	S_{IV}	$3.0\,S_m$	441

5 Conclusion

The upper fast control coil is selected and divided into two parts to perform the electromagnetic analysis. The toroidal magnetic field on the large arc segment is much larger than the radial and axial magnetic fields, but it scarcely induces Ampere force. Thus, the radial and axial load induced by the corresponding magnetic field is dominated. However, for the feeder, the toroidal magnetic field is nearly perpendicular with the current flowing through itself. Therefore, the load resulted from toroidal magnetic field is dominant. The stress on the components of fast control coil is classified and evaluated. And of which the maximum stress occurs on the conductor jacket, the peak values are not beyond the threshold of acceptance criteria, which indicate the fast control coil still has enough strength to withstand the electromagnetic force after it is updated.

Acknowledgements

This project has been financially supported by the National Magnetic Confinement Fusion Science Program of China (Grant No. 2014GB105002) and Natural Science Foundation of Guangdong Province (Grant No. 2017A030310640).

References

[1] C. NEUMEYER, A. BROOKS, L.BRYANT, et al. (2011). Design of the ITER in-vessel coil[J]. *Fusion science and technology*, Vol. 60, No. 1, pp. 95-99. AMER. USA.

[2] HUANG HAIHONG, YIN MING, WANG HAIXIN. (2014). Design of controller for new EAST fast control power supply[J]. *Plasma science and technology*, Vol. 16, No. 11, pp. 1068-1073. IOP. England.

[3] XIAO B. J., HUMPHREYS D. A., WALKER M. L. et al. (2008). EAST plasma control system[J]. *Fusion engineering and design*, Vol. 83, No. 2-3, pp. 181-187. ELSEVIER. Netherlands.

[4] SHIJUN DU, XUFENG LIU. (2008). Design and fabrication of the active feedback control coils for EAST[J]. *Fusion engineering and design*, Vol. 83, No. 5-6, pp. 766-770. ELSEVIER. Netherlands.

[5] D.M. YAO, J.G. LI, Y.T. SONG et al. (2005). EAST in-vessel components design[J]. *Fusion engineering and design*, Vol. 75-79, pp. 491-494. ELSEVIER. Netherlands.

[6] LONG FENG, WU YU, DU SHIJUN et al. (2013). Manufacture of EAST VS In-Vessel Coil[J]. *Fusion engineering and design*, Vol. 88, No. 12, pp. 3194-3198. ELSEVIER. Netherlands.

[7] DAMAO YAO, GUANGNAN LUO, SHIJUN DU et al. (2015). Overview of the EAST in-vessel components upgrade[J]. *Fusion engineering and design*, Vol. 98-99, pp. 1692-1695. ELSEVIER. Netherlands.

[8] YUESEN CHU. (1999). Numerical Calculation for the Magnetic Field in Current-Carrying Circular Arc Filament[J]. *IEEE transactions on magnetics*, Vol. 27, No. 6, pp. 1588-1595. IEEE. USA.

[9] LAXMIKANTK, URANKAR. (1980). Vector Potential and Magnetic Field of Current-Carrying Finite Arc Segment in Analytical Form. 1. Filament Approximation[J]. *IEEE transactions on magnetics*, Vol. 16, No. 5, pp. 1283-1288. IEEE. USA.

[10] QIULIANG WANG. (2007). High magnetic field superconducting magnet science[M]. pp. 47-53. *Science Press*, China.

[11] LAXMIKANTK, URANKAR. (1982). Vector Potential and Magnetic Field of Current-Carrying Finite Arc Segment in Analytical Form. 3. Exact Computation for Rectangular Cross-section [J]. *IEEE Transactions on Magnetics*, Vol. 18, No. 6, pp. 1860-1867. IEEE. USA.

[12] LAXMIKANTK, URANKAR. (1990). Vector Potential and Magnetic Field of Current-Carrying Finite Arc Segment in Analytical Form. 5. Polygon Cross-section [J]. *IEEE Transactions on Magnetics*, Vol. 26, No. 3, pp. 1171-1180. IEEE. USA.

[13] VITUPIER G, MEEKINS M, SBORCHIA C, et al. (2015). ITER cryostat structural analysis. 2015 *IEEE 26th Symposium on Fusion Engineering*, 2015 May 31-June 4, Austin, USA.

[14] PECHÁČ PETER, SÁGA MILAN, SAPIETA MILAN. (2018). Numerical simulation of cold rolled steel sheet metal during blanking process[J]. *Manufacturing Technology*, Vol. 18, No. 3, pp. 462-465. Engineering Village. USA.

[15] SONTAMINO, ARKARAPON, PHANITWONG, WIRIYAKORN. (2017). Finite element analysis of counterbore-shaped parts by using sheet-bulk metal forming process[J]. *Manufacturing Technology*, Vol. 17, No. 4, pp. 597-602. Engineering Village. USA.

[16] VAVRO JÁN, KOVÁČIKOVÁ PETRA, BEZDEDOVÁ RADKA, HÍREŠ JAKUB. (2017). Kinematic and dynamic analysis and distribution of stress in items of planar mechanisms by means of the MSC ADAMS software[J]. *Manufacturing Technology*, Vol. 17, No. 4, pp. 597-602. Engineering Village. USA.

10.21062/ujep/264.2019/a/1213-2489/MT/19/1/172